China Ocean Engineering, Vol.17, No.1, pp.45 – 60

Nearshore Wave Field Analysis Using SAR Images[1]

DOONG Dongjiing[a,*], KAO Chiachuen[a]
CHUANG Zsuhsin[b] and LIN Hongpeng[a]

[a] *Department of Hydraulics and Ocean Engineering, Cheng Kung University, Tainan 701, China*
[b] *Coastal Ocean Monitoring Center, Cheng Kung University, Tainan 701, China*

(Received 12 July 2001; received in revised form 28 November 2002; accepted 15 December 2002)

ABSTRACT

Satellite remote sensing technique offers a wide range of information, and is one of the tools for ocean wave observation. This paper discusses the limitations of Synthetic Aperture Radar (SAR) images in wave field analysis. It is found that the wave field analysis is affected by the gray value distribution of image and the relationship between satellite travel and wave propagation directions. Since human activities and coastal engineering are performed in nearshore areas, some issues are discussed for nearshore SAR image analysis. Several case studies show that the wave parameters estimated from nearshore SAR images are quite different from in-situ measurements, suggesting that the wave information derived from nearshore SAR images cannot appropriately represent the wave characteristics. One of the reasons is that the wave field is non-homogeneous in the nearshore area.

Key words: *SAR image*; *directional wave spectra*; *nearshore*; *wave field*

1. Introduction

Ocean waves, which are extremely random, are directly and indirectly dependent on meteorological, hydrological, oceanographical and topographical factors. They cannot be fully understood only by theoretical approaches. Field measurement must be performed to increase the knowledge of them. Diverse ways of wave measurement have been developed and adopted for specific purposes and conditions in the past few decades. They may be categorized into In-Situ measurement and Remote Sensing Techniques. Various techniques of in-situ measurement have been developed and improved, but most of them are confined to space limitation. The remote sensing approach then demonstrates its considerable potential in providing space information on directional random waves, even if there is a severe sea-state.

Many studies had taken the advantage of airborne data collection even before the United States launched the SEASAT satellite in 1978 (Gonzales *et al.*, 1979). Many more resource satellites that had been launched by the 1990's offered higher resolution images of the sea surface. The Synthetic Aperture Radar (SAR) is a side-looking imaging radar operating from a moving platform. SAR images of the Earth's surface represent the spatial pattern of reflected microwave energy. A series of electromagnetic pulses is transmitted towards the Earth in a direction perpendicular to the platform track. The pulses illuminate an elliptical footprint on the Earth's surface owing to the directional properties of the

1 This study was supported by NSC in Taiwan under the project No. NSC 89-2611-E-006-040.
* Corresponding author; E-mail: djdoong@pchome.com.tw

antenna. The strength of the signal returning from the area covered by the footprint depends upon the physical characteristics of the surface. The amount of energy reflected from a point target is given by the radar cross section (RCS) defined as the projected area of a metal sphere that returns the same echo signal as the target. Quantifying the cross-sectional values makes it possible to relate the returned energy to the physical properties of the scene.

SAR provides all weather images of the sea surface topography during day and night. Many oceanographic processes and phenomena can be observed by SAR, such as internal waves, wind signatures, oceanic fronts, surface films, current fields, bottom topographic features, ship wakes, and mesoscale eddies, via their influence on the short wind waves responsible for microwave backscatter, and reported (Liu *et al.*, 1994; Hsu *et al.*, 2000). SAR image is also useful to the study of marine pollution problem, such as the monitoring of oil-polluted area (Wu *et al.*, 1998). In addition, SAR image is used to estimate the surface wave field, such as wave height, period, direction and wavelength. These wave parameters are calculated from wave spectrum. However, the spectrum derived from SAR image is called the image spectrum that is not real ocean wave spectrum. The modulation transfer function (MTF) that relates to the imaging mechanisms such as hydrodynamics of modulation, tilt modulation, and velocity bunching should be applied to transfer the image spectrum to wave spectrum. MTF is still not that well understood (Hasselmann *et al.*, 1985; Alpers and Bruening, 1986). However, there are many studies for examining the extraction of wave field from SAR image, and applying to study the wave-current interaction problem and so on (Peng and Liu, 1995; Beal *et al.*, 1986). Most of these studies analyzed the deep water SAR images. This study is going to investigate the operation of extraction of wave field using nearshore SAR images.

Many coast engineering and human activities take place in nearshore areas. In response to the demand for high quality meteorological and oceanographic data, a monitoring network comprising data buoys and other automatic observation systems is planned and is being set-up in Taiwan by the Coastal Ocean Monitoring Center (COMC) of Cheng Kung University. Real-time in-situ data from these operational observation systems have been used for weather forecasting, model validation, engineering design, etc. Besides the in-situ measurements, COMC is attempting to collect data over broader areas using remote sensing techniques. This development seeks to extend the wave information from point to spatial observations. The objective of this study is to understand the capability of the satellite remote sensing. Some notes on wave spectrum analysis of nearshore satellite images are presented and a comparative study is described in the following sections.

2. SAR Images and Field Data

2.1 ERS-1 SAR Images

In this study, SAR images from European Remote Sensing Satellites (ERS-1/2) are used. Both ERS-1 and ERS-2 operate at 5.3 GHz (C-Band) with linear vertical polarization at an altitude of 785 km at the incidence angle of 23°. The SAR acquires high resolution images to the right of its track by transmitting and receiving the strength of electromagnetic radiation, expressed in a digital form as gray

values. The ERS-1/2 satellites orbit the earth in a north-to-south descending mode. The satellite passes over the Taiwan area at roughly 10:30 AM. Each full SAR image spans an area of around 100 km × 100 km, and all pixels are nearly square of 12.5 m by 12.5 m. The output of the SAR processor is an image that looks much like a very grainy photograph, with a dense irregular pattern of bright and dark spots.

Eight SAR images of the nearshore coastal areas around Taiwan are selected based on the following principles. First, to facilitate comparative analysis, the images must include field observation stations. Second, to obtain significant results, the wave patterns of selected SAR images must be clear. Most of the significant wave heights in the eight images selected are larger than 1.0 m. The location of the selected images is shown in Fig. 1. Five images are from coastal areas near Hualien in eastern Taiwan, two are from the Taiwan's northeastern cape, and one is from Hsinchu along the central part of the Taiwan Straits. The satellite images are shown in Figs. 2(a) ~ 2(h). The quadrate frames and the letters in parentheses in the photos delineate the sub-images used in the following sections.

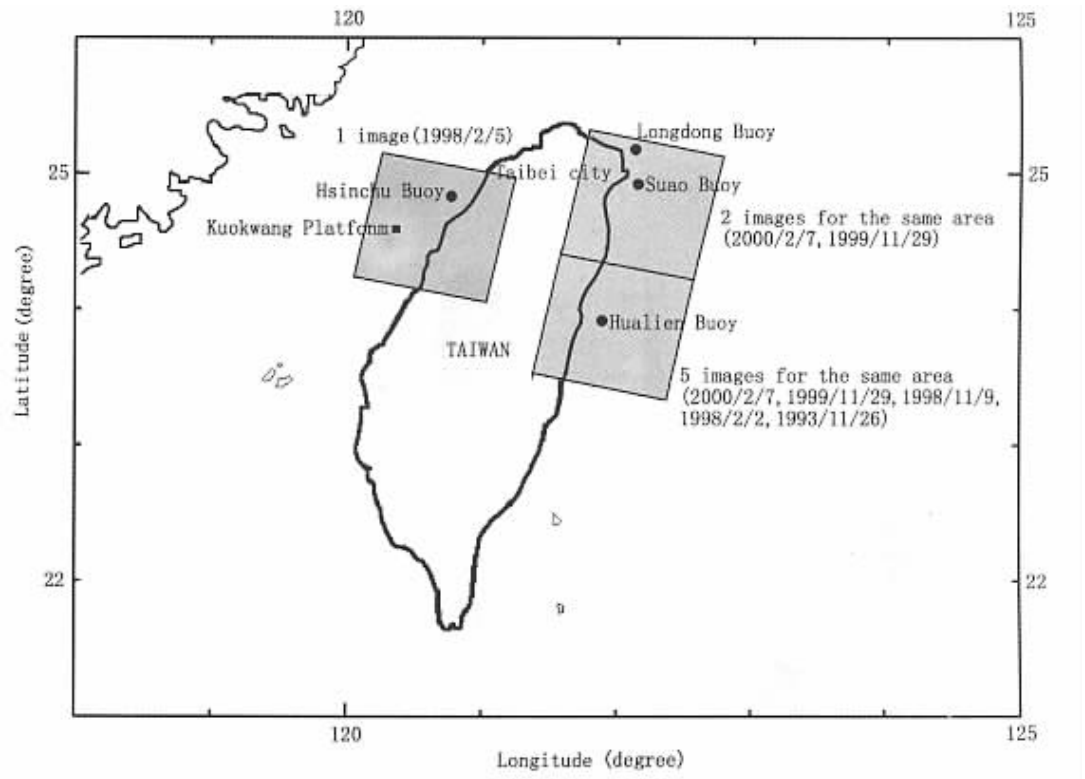

Fig. 1. The locations of the SAR images and in-situ stations.

2.2 Field Measurements

In order to verify the results of SAR image analysis, in-situ observation data are collected. The data buoy is the most frequently used instrument for oceanographic observation. It provides wave data

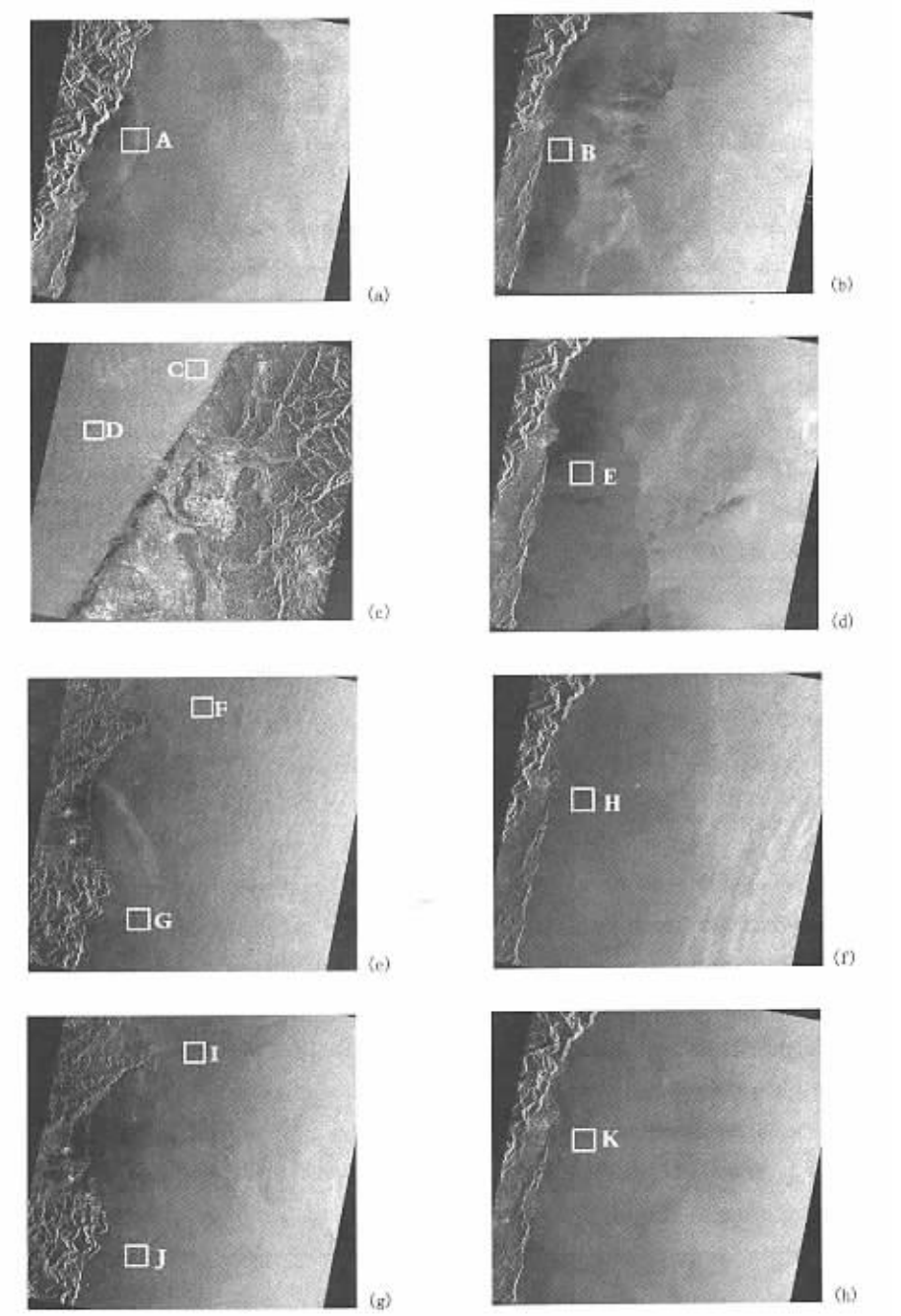

Fig. 2. SAR images.

(a). Eastern Taiwan Waters [1993/11/26] (b). Eastern Taiwan Waters [1998/2/2]
(c). Western Taiwan Waters [1998/2/5] (d). Eastern Taiwan Waters [1998/11/9]
(e). Northeastern Taiwan Waters [1999/11/29] (f). Eastern Taiwan Waters [1999/11/29]
(g). Northeastern Taiwan Waters [2000/2/7] (h). Eastern Taiwan Waters [2000/2/7]

as well as meteorological information, such as wind, barometric pressure, temperature, etc. COMC has been dedicating itself to the design, development, operation and maintenance of the data buoy system around Taiwan (Kao *et al.*, 1999). The data buoy is powered by solar energy, making it suitable for long-term operation. Batteries are used to store the energy for continuous operation during nighttime and in bad weather. To meet the need for real-time data for the forecast purpose, observation data is transmitted via radio telemetry, and in case of far remote station, via satellite, immediately after each measurement.

In this study, the data from COMC data buoys at Hsinchu, Longdong, Suao, and Hualien, as well as data from the Central Weather Bureau's Kuokwang Platform offshore of Hsinchu are used. The buoys are located in nearshore waters at a depth of approximately 30 m, while the Kuokwang Platform is located nearly at the centre of the Taiwan Straits at a depth of 60 m. The data from these observation stations is shown in Table 1.

Table 1 The SAR images and corresponding sea state at the in-situ stations

Image No.	Locations of SAR images	Date of SAR images received	In-Situ Stations	In-situ measurements			Case No.
				Significant wave height (cm)	Significant wave period (sec)	Wave direction (°)	
1	Eastern Taiwan Waters	1993/11/26	Hualien Waverider	166	8.4	96	A
2	Eastern Taiwan Waters	1998/02/02	Hualien Buoy	122	6.6	45	B
3	Western Taiwan Waters	1998/02/05	Hsinchu Buoy	221	5.8	0	C
			Kuokwang Platform	287	6.5	-	D
4	Eastern Taiwan Waters	1998/11/09	Hualien Buoy	142	8.2	90	E
5	Northeastern Taiwan Waters	1999/11/29	Longdong Buoy	96	6.7	79	F
			Suao Buoy	167	7.0	68	G
6	Eastern Taiwan Waters	1999/11/29	Hualien Buoy	162	6.0	56	H
7	Northeastern Taiwan Waters	2000/02/07	Longdong Buoy	158	5.9	45	I
			Suao Buoy	142	7.1	101	J
8	Eastern Taiwan Waters	2000/02/07	Hualien Buoy	145	5.9	112	K

3. SAR Spectrum Processing

Satellite images record the two-dimensional distribution of back scattering strength of satellite radar echoes of the sea surface. A two-dimensional fast Fourier transform (2D FFT) is used to convert these signals into wave spectral information. Eq. (1) is the FFT used.

$$F(k_x, k_y) = \frac{1}{n}\sum_{n_i=0}^{N-1}\sum_{n_j=0}^{N-1} G(n_i, n_j)\exp[-2\pi i(k_x n_i + k_y n_j)/N]. \quad (1)$$

In this equation $G(n_i, n_j)$ is the digital gray value of the pixel located at coordinates (n_i, n_j);

k_x is the wavenumber in direction x; k_y is the wavenumber in direction y; and $N = 2^r$ (r = 1, 2, 3 …) is the number of pixels on each side of the selected sub-image. This 2D FFT is used to derive the Fourier coefficients. $F(k_x, k_y)$ is a complex function, the square of which can be used to derive the wavenumber spectrum $S(k_x, k_y)$, which in turn allows the wave energy and wavelength distribution in the x-y perpendicular coordinate plane to be obtained.

The directional spectrum is the spectral energy expressed in terms of directional and frequency distribution. It is therefore necessary to change the two-dimensional perpendicular coordinate wavenumber spectrum into a polar coordinate wavenumber spectrum. The idea to convert wavenumber spectra into directional wave spectra using a dispersion relationship equation used by Leu (1998) and Kuo *et al*. (1999) is adopted in this study, as shown in Eqs. (2) and (3):

$$S(k, \theta) = S(k_x, k_y) \cdot K; \tag{2}$$

$$S(f, \theta) = S(k, \theta) \cdot \frac{\mathrm{d}k}{\mathrm{d}f}. \tag{3}$$

$S(f, \theta)$ in the above equation is the directional wave spectrum. The wavenumber-direction spectrum obtained from Eq. (2) can be used to derive the primary wavelength and wave direction. This paper defines the due north as 0°, with the angle increasing in a clockwise direction. A wave direction of 180° therefore means the wave is propagating from the south to the north. The primary wavelength is calculated as $L = 2\pi/K$. In addition, the directional spectrum derived from Eq. (3) can be used to obtain a one-dimensional frequency spectrum after integration along the directional axis, which yields the peak frequency.

In this study, a computer program based on Eqs. (1) ~ (3) is developed to calculate the directional spectrum of the SAR image. A comparison of the outcomes with reference research is made first. The SAR image of the Hualien coast on November 26, 1993, which was analyzed by Leu (1998), is used to test the accuracy. In his research, the 2D FFT with a 128 × 128 pixel sub-image is used to calculate directional spectra. A moving average scheme was taken of the image data before application of the FFT, and the resulting directional spectra are derived through the sample averaging of 16 sub-images in the vicinity of each other. A similar algorithm is used in this study, but without the sample averaging process. In addition, the differential dispersion equation, i.e. Eq. (4), is used in Eq. (3) for application of the algorithm to nearshore areas.

$$\frac{\mathrm{d}k}{\mathrm{d}f} = \frac{4\pi\sqrt{gk\tanh(kh)}}{[gk\tanh(kh) + kgh\,\mathrm{sech}^2(kh)]}. \tag{4}$$

The derived directional spectrum is shown in Fig. 3. The comparison with Leu's (1998) result is given in Table 2. It is shown that the primary wavelength and direction derived here and that by Leu (1998) are close. However, there are small differences between in-situ measurements and this study, verifying the correctness of the analytical procedures.

Table 2 Comparison of wave parameters derived in this study with Leu's (1998)

	Field data	This study		Leu (1998)		Difference between this study and Leu's (1998)
		Results	Difference from field data	Results	Difference from field data	
Wavelength (m)	132.0	137.2	5.2	149.0	17.0	11.8
Wave direction (°)	96.0	121.0	25.0	125.0	29.0	4.0
Peak wave period (sec)	10.0	10.8	0.8	10.9	0.9	0.1

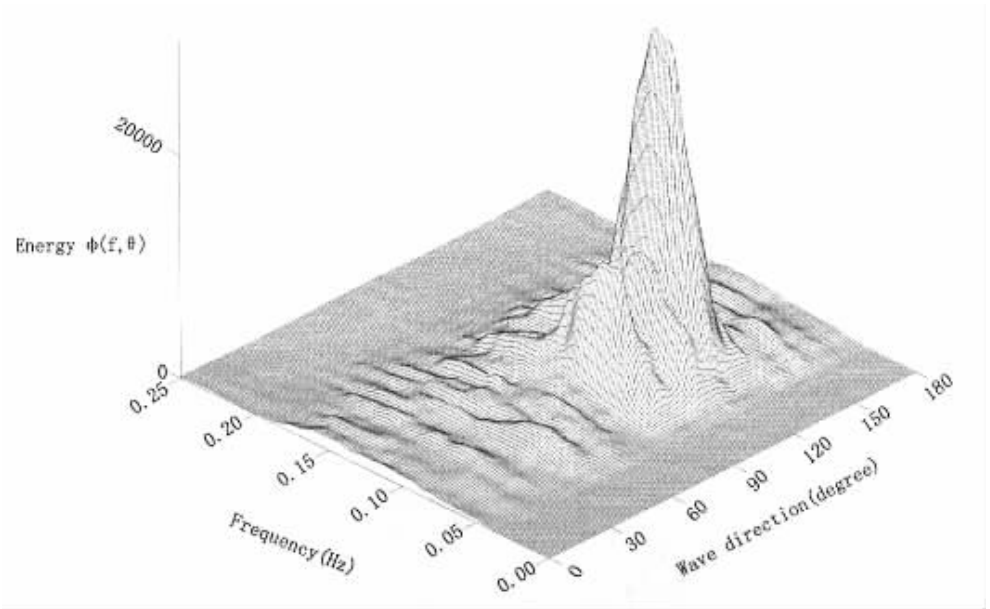

Fig. 3. Directional wave spectra derived from SAR sub-image [A] with the procedure presented in this study.

4. Limitations of the Use of SAR Images for Analysis of Ocean Waves

4.1 Effect of Distribution of Image Gray Values

Eleven sub-images in the vicinity of in-situ stations are analyzed. The derived wavenumber spectra indicate that for four of the sub-images the wave field cannot be derived (see Fig. 4). Because the directional spectra are derived from the satellite images by conversion of backscatter signals, the first thought on this problem is the characteristics of the backscatter signals.

The gray value distributions of the 11 sub-images are shown in Fig. 5. The horizontal axis is the image gray value, while the vertical axis is the probability of distribution. The dotted gray value distributions are from the images from which the wave field cannot be derived. The solid gray value distributions are from the images from which the wave field can be derived. It is found that sub-images that

cannot be analyzed have a broad gray value distribution, while those that can be analyzed have a narrow and sharp gray value distribution. Several offshore sub-images are analyzed and similar results yielded, meaning that the images for both the shallow and deep water are affected by gray value distribution.

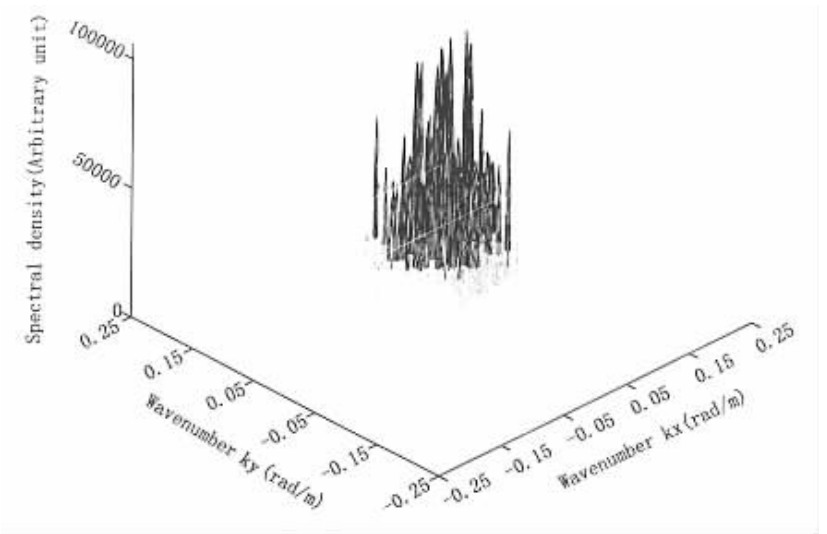

Fig. 4. An example of wavenumber spectra of non-performable sub-image.

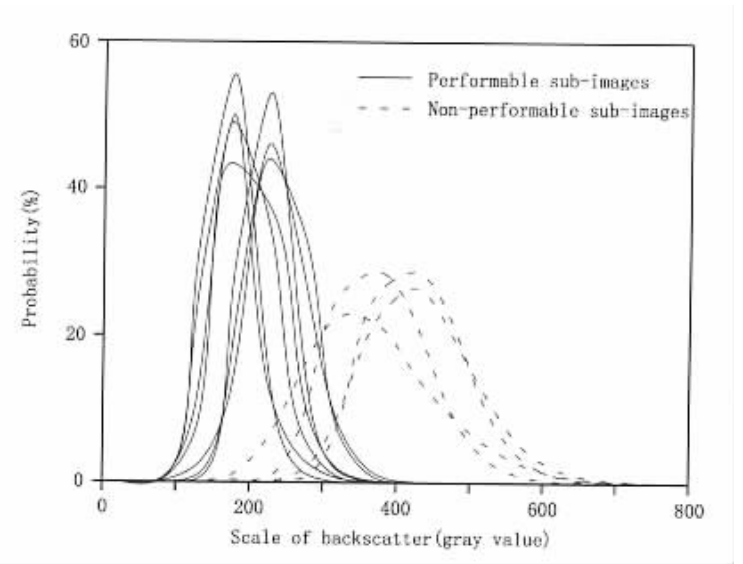

Fig. 5. Distributions of gray values of performable and non-performable images.

4.2 Effect of Relationship Between Satellite Travel and Wave Propagation Direction

Besides the effect of gray level distribution, it is found the image spectral analysis is also affected by the relationship between satellite travel and wave propagation directions. The wavelength differences

between in-situ measurements and those derived from 11 sub-images are shown in Fig. 6. The length of the bar indicates the quantitative difference. The locations of the bars in the circle represent the real wave propagation direction. ∞ in the outermost circle means that the SAR images cannot be processed. The results show that the closer the wave propagation and satellite travel, the greater the difference between measurements and those derived from SAR. Similar results have been obtained concerning wave direction. The outcomes verify the theoretical result presented by Alpers and Bruening (1986) that SAR has less performance when the wave propagation direction is parallel to satellite track.

The ERS-1/2 satellites pass Taiwan in a clockwise angle of 12.9° from the north. The long-term statistical field data show that the wave direction in the waters off western Taiwan is mostly clustered around ±22.5°, as shown in Fig. 7. This wave direction is nearly parallel to the satellite travel direction. On the other hand, the wave direction off the eastern coast of Taiwan is generally in the range of 70 ~ 110°. It is concluded that ERS SAR images of the Hualien area in eastern Taiwan are more likely to allow the determination of wave field than images of the waters off Hsinchu in western Taiwan.

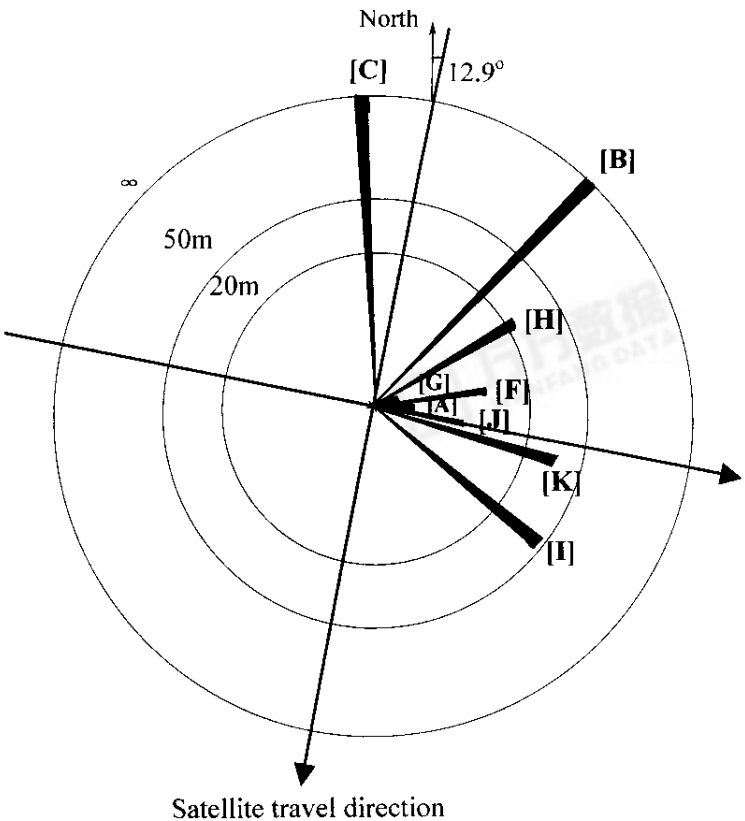

Fig. 6. The wavelength difference between in-situ measurements and those derived from SAR images for different ocean wave propagation directions.

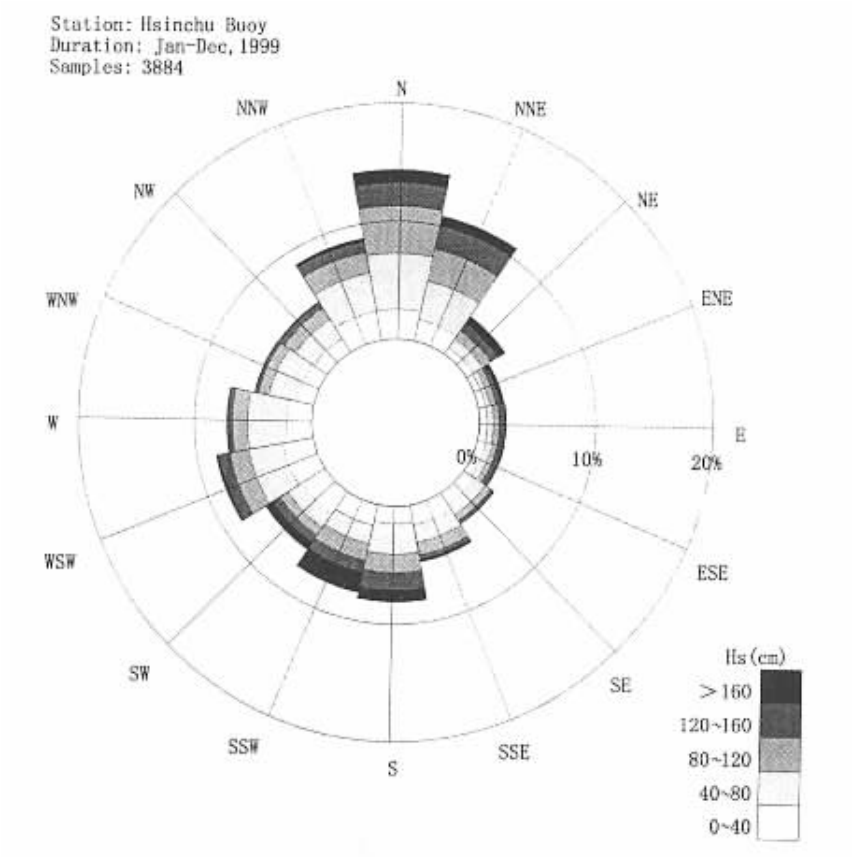

Fig. 7. Wave height-direction rose diagram of the field data from waters off Hsinchu in western Taiwan.

5. Use of SAR Images to Analysis of Nearshore Wave Fields

Many oceanic activities and coastal engineering take place in nearshore waters. This section will discuss the techniques for using nearshore SAR images to the derivation of directional spectra. A comparison of SAR and in-situ measurements will be made. The aforementioned 11 sub-images and corresponding data from nearby in-situ stations are given the designations A through K, as shown in Table 1.

5.1 Some Notes on the Applications

5.1.1 *Selection of Sub-Image Size*

In general, the sub-image is cut from the full size SAR image for wave spectral analysis. The derivation of image spectrum is therefore affected by the size of the sub-image. A small sub-image may contain insufficient wave information, however, a large sub-image may not meet the hypothesis of homogeneity. Beal *et al.* (1986) chose to analyze 512×512 pixel sub-images, but those images are all deep ocean related. Since this study aims to analyze images for shallow waters, the above image size is not necessarily appropriate.

Eleven 512×512 pixel sub-images are selected for spectral analysis, as shown in Fig. 2. Each

sub-image contains an in-situ station. Sub-images of several different sizes (64×64, 128×128, 256×256, 512×512 pixel) are cut from each of the eleven 512×512 pixel sub-images for spectral analysis. The discrepancy of wavelength and wave direction between the derived and the field measured is used to determine the appropriate sub-image size. The reason for determining the appropriate sub-image size is small discrepancy. In addition, the uncertainty of discrepancy is the other reason. The boxplot (Fig. 8) is used to illustrate the results of analysis. The horizontal line in the box represents the mean discrepancy, while the lower and upper edges of the box indicate the 25% and 75% discrepancies respectively. The length of the box represents uncertainty. Fig. 8, shows that the mean discrepancy of the wavelength derived from the 128×128 pixel sub-image is smaller than that derived from sub-images of other sizes. The uncertainty from estimation of 128×128 pixel sub-image is also small. This leads to the choice of 128×128 pixel sub-image as the unit for analysis of nearshore SAR images.

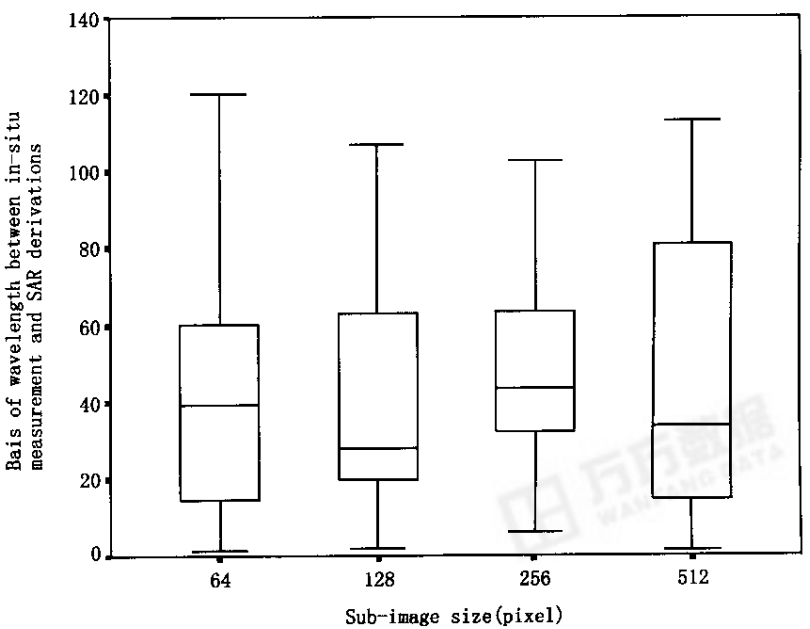

Fig. 8. Uncertainty estimation by different sub-image sizes.

5.1.2 *Discussion on Spectra Averaging Process*

The average of the spectra from several sub-images is taken for reduction of random error. Owing to the wave field changes with depth in nearshore waters, the use of the spectra averaging method may cause the error to increase. Sub-images near Hualien and Suao buoys, which respectively represent steep and mild seabed slope area, are selected. One 512×512 pixel image is divided into 16 equal 128×128 pixel sub-images. Sample averaging of the wavenumber spectra derived from these 16 sub-images is then performed. The result is shown in Table 3. It can be seen that the discrepancy from sample averaging of 16 128×128 pixel sub-images is actually greater than that of the single 128×128 pixel sub-image, implying that spectra averaging method is not appropriate in the analysis of the wave

field with nearshore images.

Table 3 Comparison of results of SAR wave field analysis with and without sample averaging technique

		Single 128 × 128 pixel sub-image	Sample averaging of 16 sub-images	Remarks
SAR sub-image for Northeastern Taiwan Waters [Case G]	Wavelength	1.6m/1.2%	22.9m/17.1%	mild seabed
	Wave direction	2°	11°	
SAR sub-image for EasternTaiwan Waters [Case K]	Wavelength	34.7m/27.2%	48.8m/42.1%	steep seabed
	Wave direction	2°	18°	

5.2 Comparison of SAR and Data Buoy Wave Fields

Since there exist some limitations in the analysis of SAR wave field, it is interesting to know the quantitative discrepancy between images and in-situ measurements. A comparison of the 11 sub-images with in-situ measurements is shown in Table 4. The analyses show that not all nearshore images can be used to wave field analysis. The average wavelength discrepancy of the seven analyzed sub-images is approximately 20 m (16%), while the average wave direction discrepancy is approximately 12°. For discussion of the range of the discrepancy for shallow and deep waters, directional spectra are also derived from deep water images. Since there are no field stations to provide comparative deep water data, the nearshore buoy data and water depth information are used to infer the wave parameters for sub-images of deep water images. A comparison of the results of SAR image analysis and those of indirect wave field derivation shows that the discrepancy for deep water areas is indeed smaller than that in nearshore cases. Although indirect derivation of wave parameters introduces another source of error, the obtained results are of a certain degree of reliability.

5.3 Effect of Non-Homogeneous Nearshore Wave Field

The traditional field wave observation method takes measurements at single points. The wave data collected in this way only represent the wave characteristics in the vicinity of that particular measuring station. Although the remote sensing image covers large sea area, each of the wave information (wave height, wavelength or wave direction) within the image is only represented by one value. This section aims to discuss the legitimacy of this representation method.

The spatial wave characteristics vary with water depth. For example, the wavelength of a long-peak wave will shorten as it moves from deep water to the nearshore area. The change of wavelength could be estimated theoretically by ocean wave dispersion equation as shown in Fig. 9. It is found that the larger the period of the wave, the more the wavelength will change as it propagates to the shore. Take waves with periods of 9.5 and 10.5 seconds as an example. The wavelength of a wave with a period of 9.5 seconds changes by approximately 50 m as the water depth changes from 60 m to 15 m, while the wavelength of a wave with a period of 10.5 seconds will change by 70 m. This result is derived under the condition of single wave propagation. However, the real ocean wave is extreme random

and it is assumed that infinite waves are contained in a remote sensing image. In addition, water depth may not vary uniformly for each propagation path. Furthermore, the wave direction is also very complex due to the effect of wave refraction and diffraction. These facts show that the wave field in the nearshore SAR image could be assumed as non-homogeneous.

Table 4 Comparison between wave parameters from SAR image analysis and field measurements

Case	SAR image analysis			In-situ measurements			Discrepancy		
	Wave length (m)	Wave direction (°)	Wave period (sec)	Wave length (m)	Wave direction (°)	Wave period (sec)	of wave length (m/%)	of wave direction (°)	of wave period (sec)
A	137.2	121	10.8	132.0	96	10.0	5.2 / 3.9	25	0.8
B	—	—	—	96.5	45	8.0	—	—	—
C	—	—	—	87.0	0	8.0	—	—	—
D	—	—	—	104.6	—	8.3	—	—	—
E	—	—	—	200.8	90	13.1	—	—	—
F	144.8	96	10.0	129.3	79	9.5	15.5 / 12.0	17	0.5
G	132.4	66	10.2	134.0	68	10.5	1.6 / 1.2	2	0.3
H	169.6	58	9.0	147.7	56	10.5	21.9 / 14.8	2	1.5
I	162.5	114	10.0	115.1	135	8.8	47.4 / 41.2	21	1.2
J	132.0	114	10.6	118.0	101	9.5	14.0 / 11.9	13	1.1
K	162.4	114	9.5	127.7	112	9.5	34.7 / 27.2	2	0.0
Mean							20.0/16.0		

Note: "—" means the sub-image is non-performable.

Two sub-images for Suao (case G) and Hualien (case H) are selected. The water depth variations for the images are 40 m (changing from -60 m to -20 m) and 100 m (changing from -130 m to -30 m) respectively, as shown in Fig. 10. The corresponding peak wave periods of in-situ measurements for cases G and H are both 10.5 seconds. From the theoretical results in Fig. 9, the sub-image in case G should contain the waves with wavelength varying from 130 m to 170 m, and the sub-image in case H, from 145 m to 170 m. For these two examples, the derived wave parameters for case G have smaller biases than for case H, as listed in Table 4. If the spatial water depth variation is used as the index of wave field homogeneity, case G and case H are assumed to be the slightly and significantly non-homogeneous images respectively. It is shown that the discrepancies of wavelength and wave direction are 1.6m and 1.2° for the slightly non-homogeneous image (case G). However, larger discrepancies are found for the significantly non-homogeneous image (case H), which are 21.9 m for wavelength and 14.8° for wave direction. These two examples verify the above discussion. Therefore, using a single parameter to represent the complex non-homogeneous wave field is challenged. Some other representative parameters should be presented to properly interpret the non-homogeneous wave field in the future study. Before the investigation on new representations, the variation of water depth should be considered in the derivation of wave parameters from nearshore images.

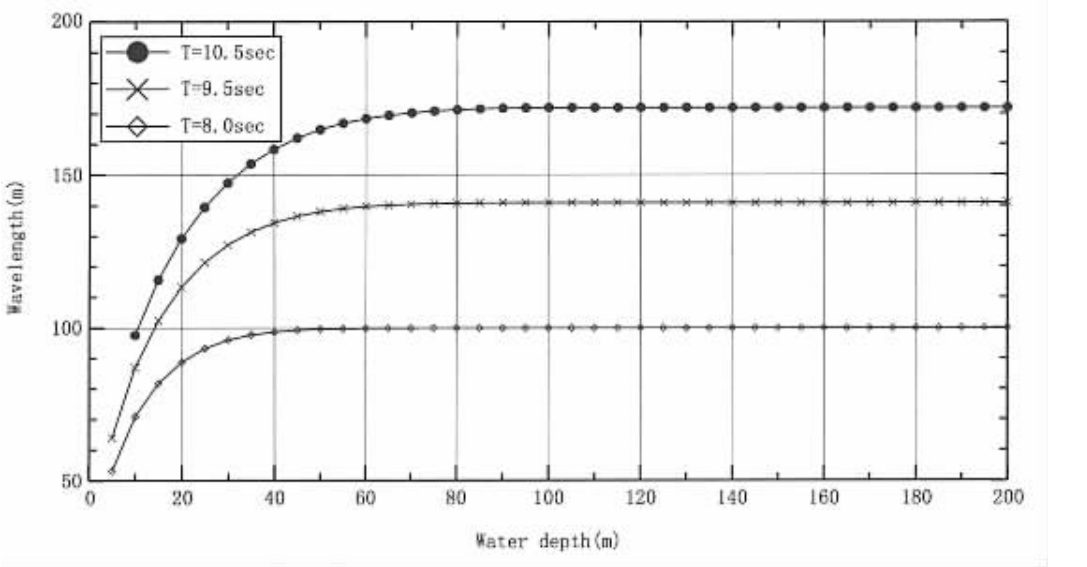

Fig. 9. Wavelength vs. water depth for different waves.

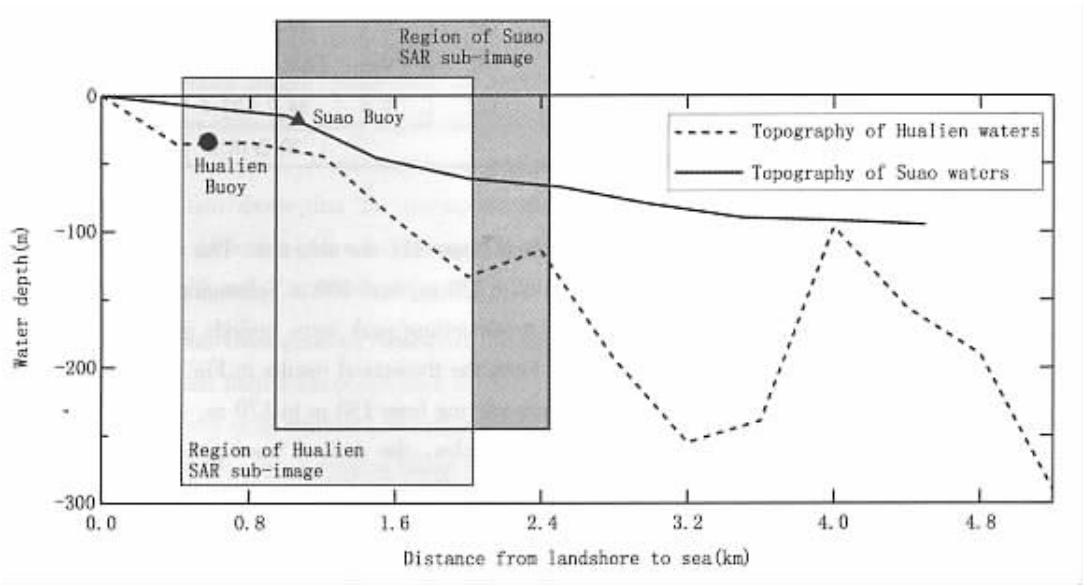

Fig. 10. Topography and SAR image locations of Hualien and Suao coast in eastern Taiwan waters.

6. Conclusions

This study investigates the applicability of SAR images to wave spectral analysis and the limiting conditions restricting their use. For a better understanding of nearshore wave field analysis with SAR images, this study discusses some issues that must be taken into consideration during the analysis of

nearshore SAR images. Comparisons are performed with in-situ data from nearby stations. The following conclusions are drawn from this process:

1. Not every SAR image can be used to the analysis of directional wave spectra. At least, the gray value distribution of images and the relationship between the direction of satellite travel and wave motion can affect the quality of analytical results.
   (1) When the distribution of image gray values is broad, it is difficult to perform image spectral analysis.
   (2) The closer the satellite travel direction to the wave prorogation direction, the larger the discrepancy between SAR and in-situ measurements.
   (3) The ERS SAR images of eastern Taiwan can better determine the wave field than the images of western Taiwan.
2. The following notes should be taken into consideration when nearshore SAR images are analyzed:
   (1) It is suggested that the sub-image size of 128 × 128 pixel be used as spectral analysis unit.
   (2) Unless the variation of water depth in the sub-image is small, the use of sample averaging to reduce FFT random error may possibly cause even larger error.
3. The results from 11 case studies show that the discrepancy in wavelength and wave direction between nearshore SAR derivation and the measured by data buoys for shallow waters is larger than that for deep waters. The differences are approximately 20 m (16%) and 12° for wavelength and wave direction, respectively.
4. The non-homogeneity of wave field within a sub-image has an important effect on SAR spectral analysis. The water depth variation must be taken into consideration in the derivation of the nearshore wave field from satellite images.

Acknowledgements — The authors wish to thank Dr. Beng-Chun Lee at the Central Weather Bureau for his offering the oceanographic field data, and also Prof. Yu Yu-xiu at the State Key Laboratory of Coastal and Offshore Engineering of Dalian University of Technology for his reviewing this paper and offering helpful comments.

References

Alpers, W. R. and Bruening, C., 1986. On the relative importance of motion related contributions to the SAR imaging mechanism of ocean surface waves, *IEEE Transactions on Geosciences and Remote Sensing*, GE-24, 873 ~ 885.

Beal, R. C., Gerling, T. W., Irvine, D. E., Monaldo, F. M. and Tilley, D. G., 1986. Spatial variations of ocean wave directional spectra, *Journal of Geophysics Research*, **91**(C2): 2433 ~ 2449.

Gonzales, F. I., Beal, R. C., Brown, W. E., Releonibus, P. S., Sherman, J. S., Gowere, J. F. R., Lichy, D., Ross, D. B. and Shuchman, R. A., 1979. SEASAT synthetic aperture radar: Ocean wave detection capabilities, *Science*, **204**, 1418 ~ 1521.

Hasselmann, K., Raney, R. K., Plant, W. J., Alpers, W., Shuchman, R. A., Lyzenga, D. R., Rufenach, C. L. and Tucker, M. J., 1985. Theory of synthetic aperture radar ocean imaging: A MARSEN view, *Journal of Geophysics Research*, **90**, 4659 ~ 4686.

Hsu, M. K., Liu, A. K. and Liu, C., 2000. A study of internal waves in the China Seas and Yellow Sea using SAR, *Continental Shelf Res.*, 20, 389 ~ 410.

Kao, C. C., Chuang, Laurence Z. H., Lin, Y. P. and Lee, B. C., 1999. An introduction to the operational data

buoy system in Taiwan, *Proceedings of International Conference on the Mediterranean Coastal Environment (MEDCOAST)*, Antalya, Turkey, 33 ~ 39.

Kuo, Y. Y., Leu, L. G. and Kao, I. L., 1999. Directional spectrum analysis and statistics obtained from ERS-1 SAR wave images, *Ocean Engineering*, **26**, 1125 ~ 1144.

Liu, A. K., Peng, C. Y. and Schumacher, J. D., 1994. Wave-current interaction study in the Gulf of Alaska for detection of eddies by SAR, *Journal of Geophysics Research*, **99**, 10075 ~ 10085.

Leu, L. G., 1998. Spectrum analysis of ocean surface wave and coastal depths derived from satellite images, *Ph. D. Thesis*, *University of Chiao Tung*, Hsinchu, Taiwan.

Peng, C. Y. and Liu, A. K., 1995. SAR observations of interaction of ocean swell and Semidi Inlands in the Gulf of Alaska, *International Journal Remote Sensing*, 16, 1249 ~ 1260.

Wu, S. Y., Liu, A. K. and Tseng, W. Y., 1998. Wavelet analysis of satellite imagery on coastal oil spills, *Proceedings of International Offshore and Polar Engineering Conference (ISOPE '98)*, 25 ~ 29.